Journal of Sound and Vibration (1998) **215**(2), 273–296
Article No. sv981612

STRUCTURAL VIBRATION CONTROL USING PZT PATCHES AND NON-LINEAR PHENOMENA

P. F. Pai

Department of Mechanical and Aerospace Engineering, *University of Missouri-Columbia*, *Columbia*, *MO* 65211, *U.S.A.*

B. Wen, A. S. Naser and M. J. Schulz

Department of Mechanical Engineering, *North Carolina A&T State University*, *Greensboro*, *NC* 27411, *U.S.A.*

(*Received* 16 *September* 1997, *and in final form* 4 *March* 1998)

We investigate non-linear saturation control, non-linear internal resonance control, and linear position-feedback control of steady-state and transient vibrations of a cantilever beam by using PZT (lead zirconate titanate) patches as actuators and sensors. The saturation control method uses the saturation phenomenon to suppress steady-state vibrations of a dynamical system with quadratic nonlinearities and 2:1 internal resonances. The internal resonance control method uses the energy exchange phenomenon due to internal resonances and added dampings to suppress transient vibrations. To test these control techniques in an efficient and systematic way, we built a digital control system that consists of SIMULINK modelling software and a dSPACE DS1102 controller in a pentium computer. Both numerical and experimental results show that the saturation control method is robust and efficient in suppression steady-state resonant vibrations. The linear position-feedback control is more robust, efficient, and convenient than the internal resonance control in suppressing transient vibrations, but it is not as robust as the saturation control in suppressing steady-state vibrations. A hybrid controller consisting of a saturation controller and a position-feedback controller is shown to be robust and efficient in controlling both transient and steady-state vibrations.

1. INTRODUCTION

In weakly nonlinear systems, internal resonances may occur if the linear natural frequencies are commensurate or nearly commensurate, and internal resonances provide coupling and energy exchange among the vibration modes [1, 2]. If two natural frequencies of a system with quadratic nonlinearities are in the ratio 2:1, there exists a saturation phenomenon [1]. When the system is excited at a frequency near the higher natural frequency, the structure responds at the frequency of the excitation and the amplitude of the response increases linearly with the amplitude of the excitation. However, when the high-frequency modal amplitude reaches a critical value, this mode saturates and all additional energy added to the system by increasing the excitation amplitude overflows into the low-frequency mode.

Recently the use of internal resonance and saturation phenomena in nonlinear control has been extensively studied [3–6]. This method is based on an approach originally introduced by Golnaraghi [3] and thoroughly investigated in reference [5]. To control transient vibrations, reference [3] used a second-order controller coupled to a vibration system via quadratic or cubic terms. References [4, 5] used the saturation phenomenon to successfully control the motion of a d.c. motor with a rigid beam attached. These control

0022–460X/98/320273 + 24 $30.00/0

techniques exploit modal interaction and saturation phenomena to transfer energy from a vibrating system to one or more electronic circuits. The control strategy is to use a linear second-order controller coupled to the vibration system via quadratic nonlinear terms (or other higher-order terms). The nonlinear terms act as an energy bridge to establish a state of exchange of energy between the system and the controller, resulting in a beating phenomenon in the response of the combined system. For controlling transient vibrations, the beating phenomenon is used to channel energy from the system to the controller and then the energy is dissipated by adding dampings before it has the opportunity to revert back to the system (called internal resonance control). For controlling steady vibrations, the controller is used as a continuous vibration absorber (called saturation control).

Aerospace structures are required to be light in weight and hence composite structures are increasingly used. Moreover, aerospace composite structures (e.g. helicopter rotor blades) are often designed with built-in elastic bending–torsion couplings to improve aerodynamic efficiency. To actively control such structures without too much added weight, PZT actuators and sensors are attractive because of their mechanical simplicity, small volume, light weight, large useful bandwidth, efficient conversion of electrical to mechanical energy, ability to perform shape control, and ability to be easily integrated with the structure. However, the integrated PZT actuators need to induce twisting moments as well as bending moments in order to control coupled bending–torsion vibrations (e.g. flutter) of structures, especially structures with elastic bending–torsion couplings. PZT-induced bending vibrations and controls have been widely studied, but there are only a few studies about PZT-induced twisting vibrations and controls [7].

A beam can be twisted by integrated PZT patches arranged in different patterns to induce bi-moments. Reference [7] investigated the twisting of a beam with PZT actuators attached at 45° to the longitudinal axis of the beam to induce two bending moments (bi-moments) that are perpendicular to each other (90° bi-moments). Reference [8] studied the twisting of a beam with PZT actuators attached parallel to the longitudinal axis of the beam and at the root of the cantilever beam to induce two bending moments that are parallel but opposite to each other (180° bi-moments). For a specific aluminum beam example, reference [8] reported that the twisted angle induced by a 180° bi-moment is about 2·7 times more than that induced by a 90° bi-moment by using the same amount of PZT material. When a PZT actuator is integrated with a structure, the induced moments and forces represent a self-equilibrated stress state of the integrated structure. It follows from St Venant's principle that a system of loads having zero resultant forces and moments (i.e. a self-equilibrated stress state) produces a strain field that is negligible at a point far away from the loading end [9]. But, for highly anisotropic and heterogeneous materials, such a self-equilibrated stress state can result in nontrivial strains with long decay lengths, which are the so-called boundary-layer solutions, or extremity solutions, or eigensolutions, or transitional solutions [9, 10]. The torsional deformation in reference [8] is partly due to the restraint warping effect that increases torsional deformations by increasing the decay lengths of torsional boundary-layer solutions.

Because the saturation control method does not require decision making as some linear control methods do, it can be built using simple commercial electronic circuits [5]. Moreover, some experimental results [11] show that this nonlinear control method works even when the structure undergoes large-amplitude vibrations and the structural system becomes nonlinear. This work is to study in detail the use of PZT patches as actuators and sensors in controlling the steady-state and transient vibrations of cantilever beams using the nonlinear control methods and to compare them with some linear control methods.

2. THEORETICAL BACKGROUND

To show the use of internal resonance and saturation phenomena for vibration control, we consider the two ordinary differential equations

$$\ddot{u}_1 + 2\zeta_1\omega_1\dot{u}_1 + \omega_1^2 u_1 = g_{12}u_1u_2,$$
$$\ddot{u}_2 + 2\zeta_2\omega_2\dot{u}_2 + \omega_2^2 u_2 = g_{11}u_1^2 + F\cos(\Omega t), \tag{1}$$

where u_1 denotes the response of a second-order controller, ω_1 is the natural angular frequency of the controller, ζ_1 is the damping ratio of the controller, u_2 represents the sensor response to a single-mode vibration of the observed structure, ω_2 is the modal frequency of the structure, ζ_2 is the modal damping ratio, g_{11} and g_{12} are positive gain constants, F is the amplitude of the external excitation force and is assumed to be positive, Ω is the external excitation frequency, t is time, and $\dot{(\,)} \equiv \mathrm{d}(\,)/\mathrm{d}t$.

We follow Nayfeh and Mook [1] and use the method of multiple scales to obtain a first-order approximate solution of equation (1) as

$$u_1 = a_1\cos\left(\frac{\Omega t}{2} - \frac{\phi_1 + \phi_2}{2}\right), \qquad u_2 = a_2\cos(\Omega t - \phi_2). \tag{2}$$

The modulation equations that govern the amplitudes a_i and phase angles ϕ_i are

$$\dot{a}_1 = -\omega_1\zeta_1 a_1 + \frac{g_{12}}{4\omega_1}a_1a_2\sin\phi_1, \tag{3}$$

$$\dot{a}_2 = -\omega_2\zeta_2 a_2 - \frac{g_{11}}{4\omega_2}a_1^2\sin\phi_1 + \frac{1}{2\omega_2}F\sin\phi_2, \tag{4}$$

$$\tfrac{1}{2}(\dot{\phi}_1 + \dot{\phi}_2)a_1 = \frac{\sigma_1 - \sigma_2}{2}a_1 + \frac{g_{12}}{4\omega_1}a_1a_2\cos\phi_1, \tag{5}$$

$$\dot{\phi}_2 a_2 = \sigma_1 a_2 + \frac{g_{11}}{4\omega_2}a_1^2\cos\phi_1 + \frac{1}{2\omega_2}F\cos\phi_2. \tag{6}$$

where σ_1 and σ_2 are detuning parameters defined as

$$\sigma_1 = \Omega - \omega_2, \qquad \sigma_2 = 2\omega_1 - \omega_2. \tag{7}$$

The amplitudes α_1 and a_2 are assumed to be positive here.

2.1. FIXED-POINT SOLUTIONS

The steady-state solutions (i.e. fixed-point solutions) correspond to constant a_i and ϕ_i, i.e. $\dot{a}_i = \dot{\phi}_i = 0$ and hence

$$0 = -\omega_1\zeta_1 a_1 + \frac{g_{12}}{4\omega_1}a_1a_2\sin\phi_1, \tag{8}$$

$$0 = -\omega_2\zeta_2 a_2 - \frac{g_{11}}{4\omega_2}a_1^2\sin\phi_1 + \frac{1}{2\omega_2}F\sin\phi_2, \tag{9}$$

$$0 = \frac{\sigma_1 - \sigma_2}{2}a_1 + \frac{g_{12}}{4\omega_1}a_1a_2\cos\phi_1, \tag{10}$$

$$0 = \sigma_1 a_2 + \frac{g_{11}}{4\omega_2}a_1^2\cos\phi_1 + \frac{1}{2\omega_2}F\cos\phi_2. \tag{11}$$

When $a_1 = 0$, it follows from equations (9) and (11) that

$$a_2 = \frac{F}{2\omega_2\sqrt{\sigma_1^2 + \omega_2^2\zeta_2^2}}. \tag{12}$$

It is the linear forced response. When $a_1 \neq 0$, it follows from equations (8) and (10) and equations (9) and (11) that

$$a_1 = \sqrt{-b \pm \sqrt{b^2 - c}}, \qquad a_2 = \frac{4\omega_1}{g_{12}}\sqrt{(\omega_1\zeta_1)^2 + \tfrac{1}{4}(\sigma_2 - \sigma_1)^2}, \tag{13}$$

where

$$b = \frac{8\omega_1\omega_2}{g_{11}g_{12}}[2\zeta_1\zeta_2\omega_1\omega_2 + \sigma_1(\sigma_2 - \sigma_1)],$$

$$c = 4\left(\frac{8\omega_1\omega_2}{g_{11}g_{12}}\right)^2(\sigma_1^2 + \omega_2^2\zeta_2^2)\left[\omega_1^2\zeta_1^2 + \frac{1}{4}(\sigma_2 - \sigma_1)^2\right] - 4\frac{F^2}{g_{11}^2}. \tag{14}$$

If $b^2 - c \geqslant 0$, it follows from equation (14) that

$$F \geqslant F_1 \equiv \left|\frac{8\omega_1\omega_2}{g_{12}}\left(\sigma_1\omega_1\zeta_1 - \frac{\sigma_2 - \sigma_1}{2}\omega_2\zeta_2\right)\right|. \tag{15}$$

Also equation (14) shows that $c \geqslant 0$ corresponds to

$$F \leqslant F_2 \equiv \sqrt{F_1^2 + \frac{g_{11}^2}{4}b^2}. \tag{16}$$

When $b < 0$, the controller u_1 responds differently to three different excitation levels. They are (1) $a_1 = \sqrt{-b + \sqrt{b^2 - c}}$ if $F > F_2$ (i.e. $c < 0$), (2) $a_1 = \sqrt{-b \pm \sqrt{b^2 - c}}$ if $F_1 < F < F_2$, and (3) $a_1 = 0$ if $F < F_1$. Hence, the threshhold value of F is F_1 when $b < 0$. When $b \geqslant 0$, (1) $a_1 = 0$ if $F < F_2$ (i.e. $c > 0$), and (2) $a_1 = \sqrt{-b + \sqrt{b^2 - c}}$ if $F > F_2$ (i.e. $c < 0$). Hence, the theshhold value of F is F_2 when $b \geqslant 0$.

Equation (13) shows that (1) $a_2 = 0$ if $\zeta_1 = 0$ and $\sigma_2 - \sigma_1 = 0$ (i.e. $2\omega_1 - \Omega = 0$), (2) a_2 is proportional to $1/g_{12}$, (3) a_2 is proportional to $\Omega - 2\omega_1$ if $\zeta_1 = 0$, and (4) a_2 is independent of F (the so-called saturation phenomenon). Case (1) indicates that, even if the excitation is not at resonance (i.e. $\sigma_1 \neq 0$), a_2 can also be controlled to be zero if $\Omega = 2\omega_1$ and $\zeta_1 = 0$. Since the natural frequency ω_1 of the controller can be easily adjusted, theoretically this control method should also work for non-resonant excitations.

Equations (13) and (14) show that, if $\zeta_1 = 0$ and $\Omega = 2\omega_1$, $a_1 = \sqrt{2F/g_{11}}$ and hence a_1 is proportional to $1/\sqrt{g_{11}}$.

It follows from equations (8) and (10) that, when $a_1 \neq 0$ and $\zeta_1 = 0$, $\phi_1 = 0^\circ$ or $\phi_1 = 180^\circ$. If $\phi_1 = 0^\circ$, it follows from equation (2) that

$$u_1^2 = \frac{a_1^2}{2} + \frac{a_1^2}{2}\cos(\Omega t - \phi_2), \qquad u_1u_2 = \frac{a_1a_2}{2}\cos\frac{1}{2}(\Omega t - \phi_2) + \frac{a_1a_2}{2}\cos\frac{3}{2}(\Omega t - \phi_2). \tag{17}$$

If $\phi_1 = 180^\circ$, we have

$$u_1^2 = \frac{a_1^2}{2} - \frac{a_1^2}{2}\cos(\Omega t - \phi_2), \qquad u_1u_2 = -\frac{a_1a_2}{2}\sin\frac{1}{2}(\Omega t - \phi_2) + \frac{a_1a_2}{2}\sin\frac{3}{2}(\Omega t - \phi_2). \tag{18}$$

Moreover, equations (9) and (11) show that, when $a_1 \neq 0$ and $\zeta_1 = 0$, ϕ_2 is very close to 180° (if $\phi_1 = 0^\circ$) or 0° (if $\phi_1 = 180^\circ$) because the modal damping ratio ζ_2 is usually very small. Substituting $\phi_2 = 180^\circ$ in equation (17) yields

$$u_1^2 = \frac{a_1^2}{2} - \frac{a_1^2}{2}\cos(\Omega t), \qquad u_1 u_2 = \frac{a_1 a_2}{2}\sin\frac{1}{2}(\Omega t) - \frac{a_1 a_2}{2}\sin\frac{3}{2}(\Omega t). \tag{19a}$$

Substituting $\phi_2 = 0^\circ$ in equation (18) yields

$$u_1^2 = \frac{a_1^2}{2} - \frac{a_1^2}{2}\cos(\Omega t), \qquad u_1 u_2 = -\frac{a_1 a_2}{2}\sin\frac{1}{2}(\Omega t) + \frac{a_1 a_2}{2}\sin\frac{3}{2}(\Omega t). \tag{19b}$$

It explains why $g_{11}u_1^2$ can be used to provide an actuation force against the external excitation force $F\cos(\Omega t)$ and why $g_{12}u_1u_2$ can be used to excite $u_1(\omega_1 \simeq \Omega/2)$ and make u_1 absorb the energy from u_2. Moreover, we will show that the constant excitation $a_1^2/2$ is important for the success of this nonlinear control method.

Since equation (13) shows that setting $\zeta_1 = 0$ reduces a_2, the following system equations will be considered in simulating the saturation control of steady-state vibrations:

$$\ddot{u}_1 + \omega_1^2 u_1 = g_{12}u_1u_2U(t - t_0),$$
$$\ddot{u}_2 + 2\zeta_2\omega_2\dot{u}_2 + \omega_2^2 u_2 = g_{11}u_1^2U(t - t_0) + F\cos(\Omega t), \tag{20}$$

where $U(t - t_0)$ is a unit-step function and t_0 is the time that the controller is activated.

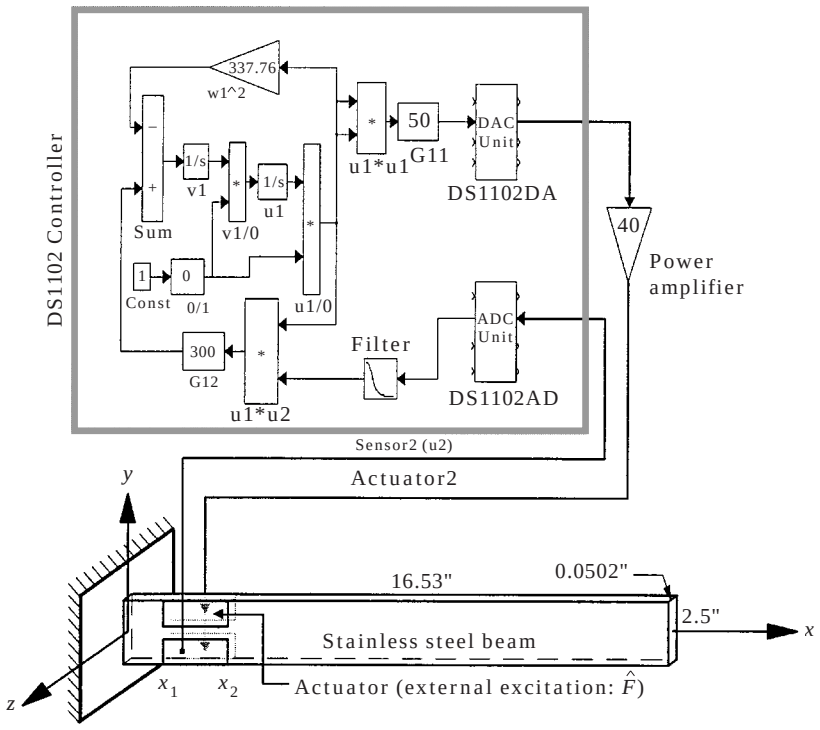

Figure 1. The cantilever beam under study and a digital saturation controller for controlling single-mode steady-state vibrations.

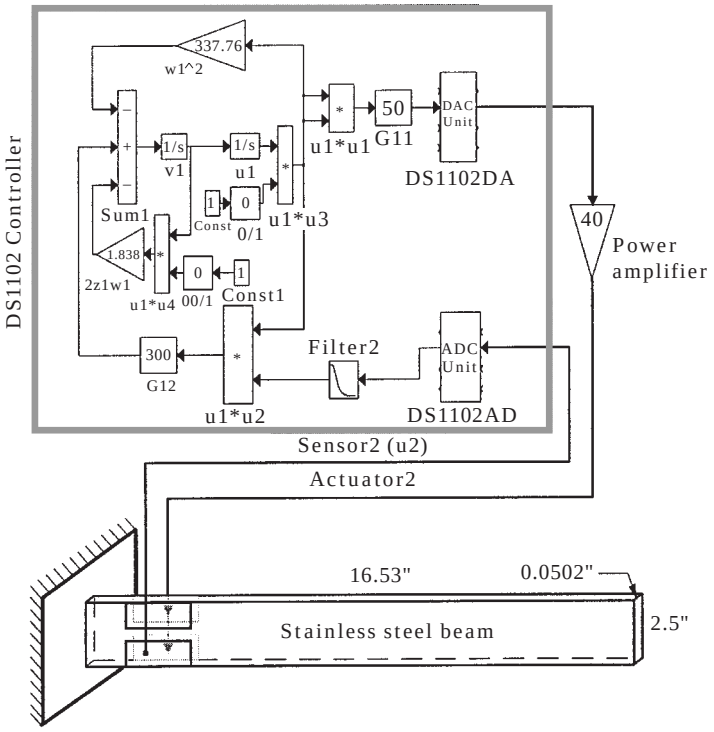

Figure 2. A digital internal resonance controller for controlling single-mode transient vibrations.

To simulate the internal resonance control of transient vibrations, the following system equation will be considered:

$$\ddot{u}_1 + 2\zeta_1\omega_1 U(t-t_1)\dot{u}_1 + \omega_1^2 u_1 = g_{12}u_1u_2, \qquad \ddot{u}_2 + 2\zeta_2\omega_2\dot{u}_2 + \omega_2^2 u_2 = g_{11}u_1^2, \tag{21}$$

where $U(t-t_1)$ is a unit-step function and t_1 is the time that the damping of the controller is turned on.

2.2. STABILITY ANALYSIS

To determine the stability of linear and nonlinear fixed-point solutions of equations (3)–(6), we need to introduce the Cartesian coordinates p_j and q_j as

$$p_1 = a_1\cos\left(\frac{\phi_1+\phi_2}{2}\right), \qquad q_1 = a_1\sin\left(\frac{\phi_1+\phi_2}{2}\right), \qquad p_2 = a_2\cos(\phi_2),$$

$$q_2 = a_2\sin(\phi_2). \tag{22}$$

Using equation (22) we reform equations (3)–(6) into

$$\dot{p}_1 = -\omega_1\zeta_1 p_1 - \frac{\sigma_1-\sigma_2}{2}q_1 + \frac{g_{12}}{4\omega_1}(q_1p_2 - p_1q_2), \tag{23}$$

$$\dot{q}_1 = -\omega_1\zeta_1 q_1 + \frac{\sigma_1-\sigma_2}{2}p_1 + \frac{g_{12}}{4\omega_1}(p_1p_2 + q_1q_2), \tag{24}$$

$$\dot{p}_2 = -\omega_2\zeta_2 p_2 - \sigma_1 q_2 - \frac{g_{11}}{2\omega_2} p_1 q_1, \tag{25}$$

$$\dot{q}_2 = -\omega_2\zeta_2 q_2 + \sigma_1 p_2 + \frac{g_{11}}{4\omega_2}(p_1^2 - q_1^2) + \frac{F}{2\omega_2}. \tag{26}$$

Because these are first-order autonomous ordinary-differential equations, the stability of a particular fixed point with respect to an infinitesimal disturbance proportional to $e^{\lambda t}$ is determined by the eigenvalues of the Jacobian matrix of the right-hand sides of equations (23)–(26). A given fixed point is stable if and only if the real parts of all eigenvalues are less than or equal to zero. If there is a pair of complex conjugate values having positive real parts, amplitude and phase-modulated motions are expected.

3. EXPERIMENTAL SET-UP

To test these control methods, we built a digital control system that consists of SIMULINK modelling software [12] and a dSPACE DS1102 controller [13] in a pentium computer. The SIMULINK software is used to build the control block diagrams, and then the dSPACE Real-Time Workshop is used to generate a C-code model from the SIMULINK model. The C-code model is then connected by the dSPACE Real-Time Interface to the dSPACE real-time hardware system for hardware-in-the-loop simulation.

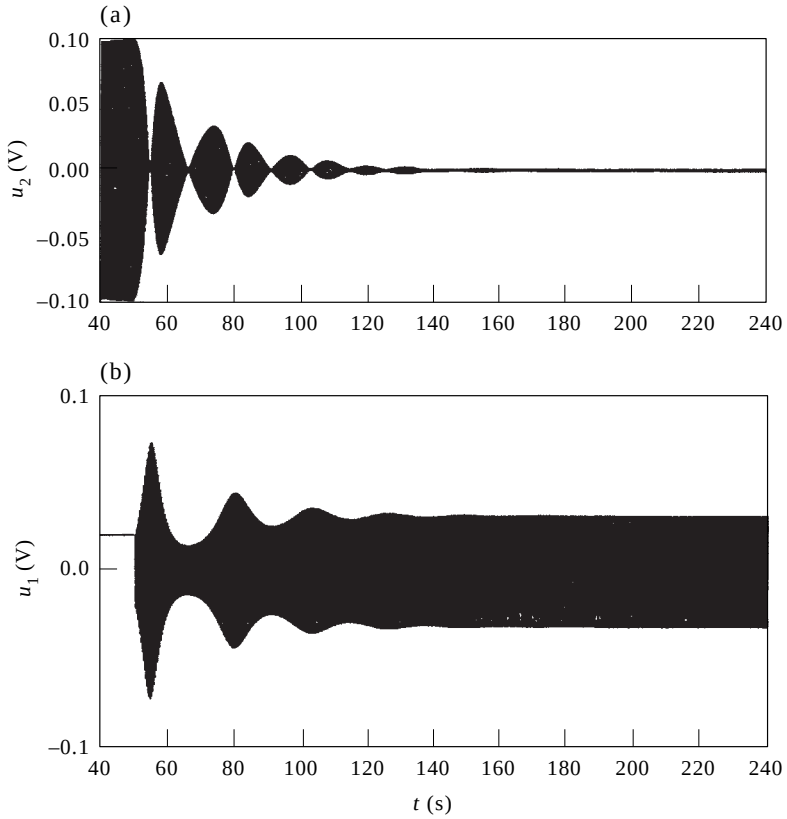

Figure 3. Theoretical saturation control of the first-mode vibration: (a) sensor response u_2 and (b) controller response u_1.

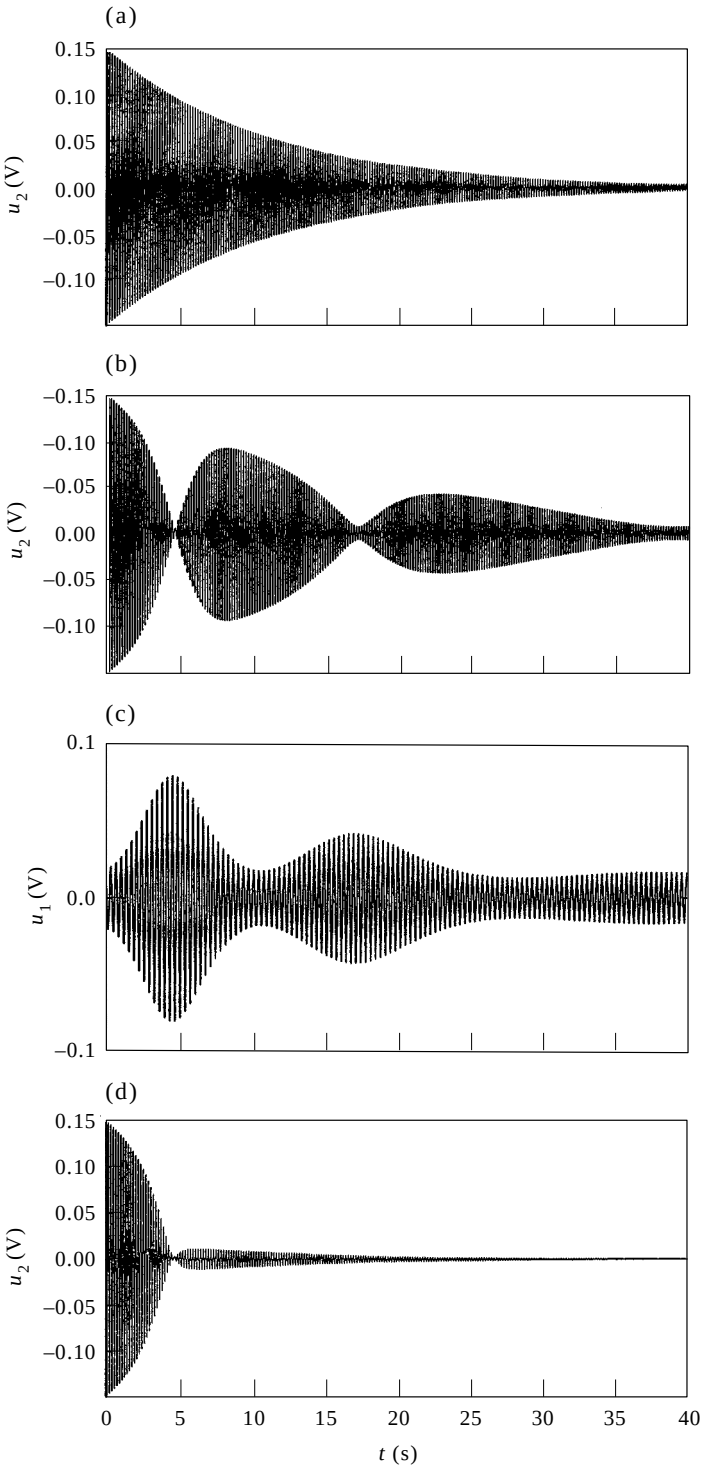

Figure 4. Theoretical internal resonance control of the first-mode transient vibration: (a) uncoupled and uncontrolled transient response u_2, (b) coupled but uncontrolled ($\zeta_1 = 0$) transient response u_2, (c) coupled but undamped controller response u_1, and (d) controlled transient response u_2.

Figure 1 shows a $16{\cdot}53'' \times 2{\cdot}5'' \times 0{\cdot}0502''$ stainless steel beam under study and the controller designed for the saturation control of the first-mode steady-state vibrations. When the variable gain "0/1" is set to zero, u_1 is disconnected from u_2. To turn on the controller, set "0/1" to one. The initial condition for "v1" (i.e. $\dot{u}_1$) is set to zero and the initial condition for "u1" (i.e. u_1) is set to a non-zero value. The filter is a Butterworth IIR low-pass filter [14] chosen from the SIMULINK library. The two pairs of PZT patches attached close to the beam root are configured to be able to control bending and torsion. This arrangement of PZT patches can be used to induce a 0° bi-moment to control bending vibrations and/or an 180° bi-moment to control torsional vibrations. However, here we only report results on the control of bending vibrations. The actuators are QP10N QuickPack PZT actuators purchased from ACX [15]. The QuickPack actuator packages piezoceramics in a protective skin (a polyimide coating) with pre-attached electrical leads. It makes fragile piezoceramics much easier to work with and easier to integrate into the structure. The actuator size is $2'' \times 1'' \times 0{\cdot}015''$. The piezo wafer size is $1{\cdot}81'' \times 0{\cdot}81'' \times 0{\cdot}01''$. Two of the PZT patches are used as actuators for control, one is used as a sensor, and one is used to provide the assumed external excitation, as shown in Figure 1. The first three natural frequencies of the beam with the four PZT patches are experimentally obtained to be 5·85 Hz, 35·22 Hz, and 97·36 Hz. The measured density is

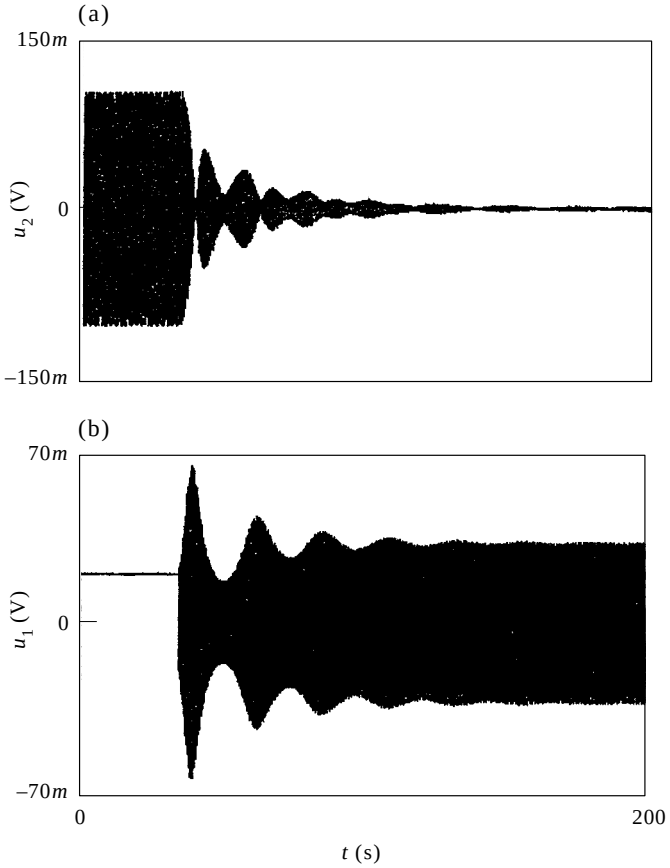

Figure 5. Experimental saturation control of the first-mode steady-state vibration: (a) time–u_2 curve, and (b) time–u_1 curve.

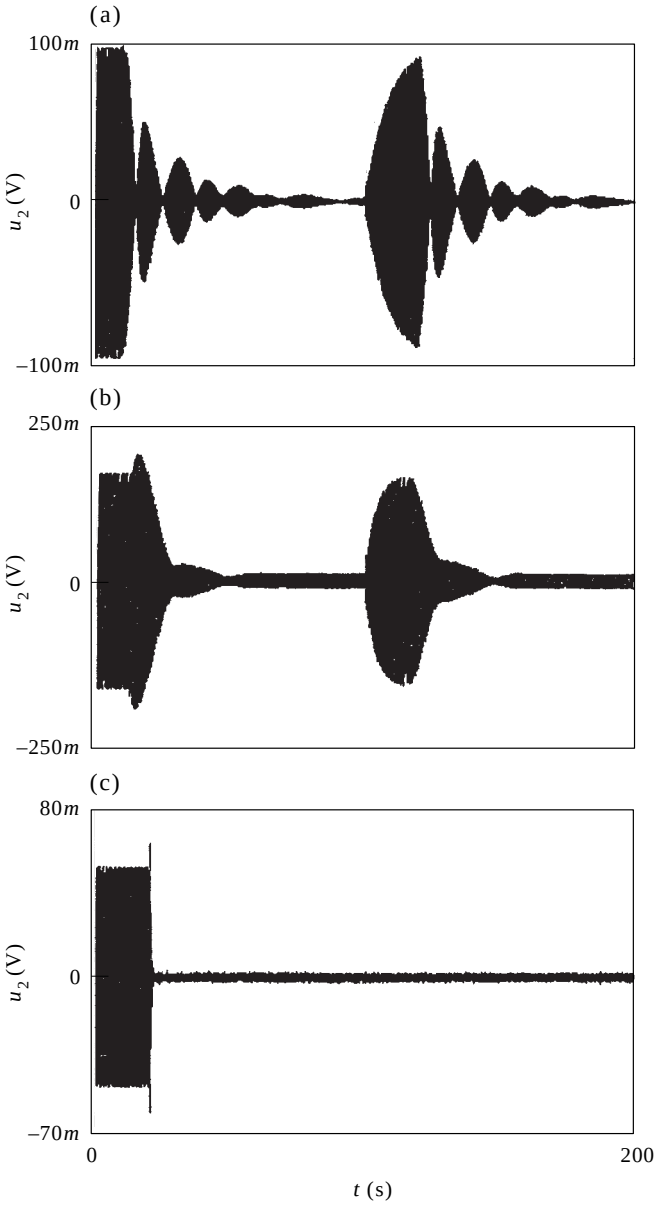

Figure 6. Experimental saturation control of steady-state modal responses u_2: (a) first-mode response, (b) second-mode response, and (c) third-mode response.

$0{\cdot}286\,\text{lb/in}^3$ and the Young's modulus is derived to be $2{\cdot}8 \times 10^7$ psi by matching the measured first natural frequency with the theoretical one.

The beam vibration is assumed to be linear according to equation (1); but when it is coupled with the controller it becomes part of a larger nonlinear system. The controller is responsible for the desirable nonlinear characteristics of the larger system. Hence nonlinear tailoring of the system is relatively straightforward and easy.

Figure 2 shows the beam with the controller designed for the internal resonance control of the first-mode transient vibrations. To couple the controller u_1 with u_2, set the gain "0/1"

to 1. To turn on the damping in u_1, set the gain "00/1" to 1. The initial condition for "v1" (i.e. $\dot{u}_1$) is set to zero and the initial condition for "u1" (i.e. u_1) is set to a non-zero value.

4. SYSTEM MODELLING AND NUMERICAL RESULTS

When a PZT actuator is not adhered to a structure, it can induce a maximum blocking stress σ_{11b} given by

$$\sigma_{11b} = E_{11}\Lambda_1, \qquad \Lambda_1 = d_{31}\frac{V_3}{t_3}, \tag{27}$$

where d_{31} is a piezoelectric strain coefficient, Λ_1 is the induced strain if the patch is free to expand, V_3 is the voltage applied across the thickness t_3, and E_{11} is the Young's modulus

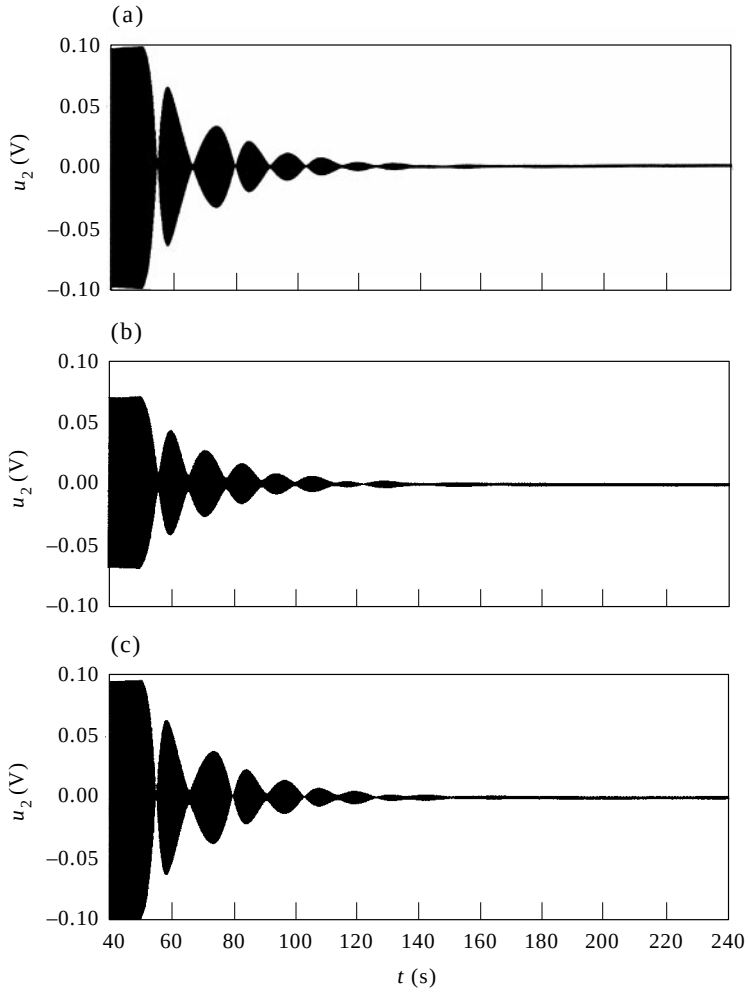

Figure 7. Theoretical saturation control of the first-mode steady-state response u_2 with non-linearities: (a) $\alpha_2 = \alpha_3 = 0$, (b) $\alpha_2 = \alpha_3 = -1000$, and (c) $\alpha_2 = \alpha_3 = 1000$.

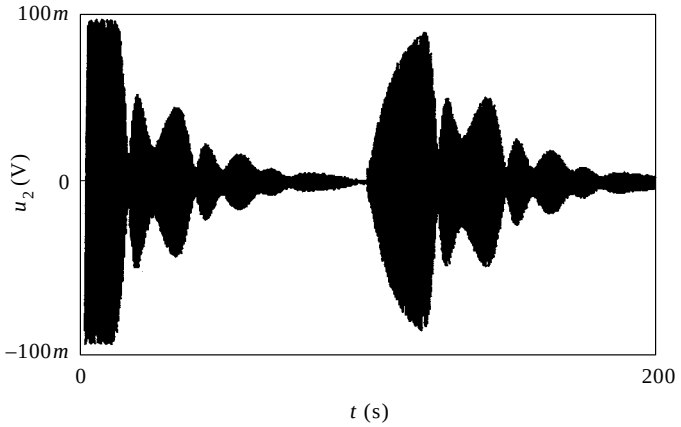

Figure 8. Experimental saturation control of the first-mode steady-state vibration using only one PZT patch for control.

of the PZT patch. When a PZT patch is used as a sensor, the induced voltage V_3 due to an applied stress σ_{11} is

$$V_3 = g_{31}\sigma_{11}t_3 = \frac{d_{31}}{K_3\varepsilon_0}\sigma_{11}t_3, \tag{28}$$

where $g_{31}(=d_{31}/K_3\varepsilon_0)$ is a piezoelectric voltage coefficient, K_3 is a relative dielectric constant, and ε_0 is the dielectric constant of vacuum space.

Unfortunately, the actual PZT-induced strains, forces, and bending moments depend on the structural material, the thickness and material properties of the adhesive layer that integrates the PZT patch with the structure, wiring, and even boundary and loading conditions. Moreover, the piezoelectric strain and voltage coefficients may not be constant under large voltages, and hysteresis and creeping under a large d.c. voltage have been reported. Hence, it requires detailed three-dimensional analysis of the coupled dynamic electrical-mechanical problem in order to have accurate results. Furthermore, manufacturers of PZT patches may not provide all the coefficients needed in using equations (27) and (28).

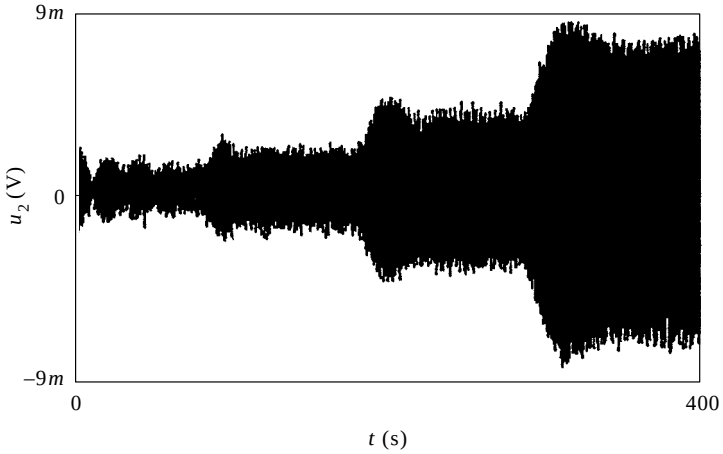

Figure 9. Controlled steady-state first-mode response u_2: $g_{12} = 400$ when $0 < t < 100$ s, $g_{12} = 200$ when $100 < t < 200$ s, $g_{12} = 100$ when $200 < t < 300$ s, and $g_{12} = 50$ when $300 < t < 400$ s.

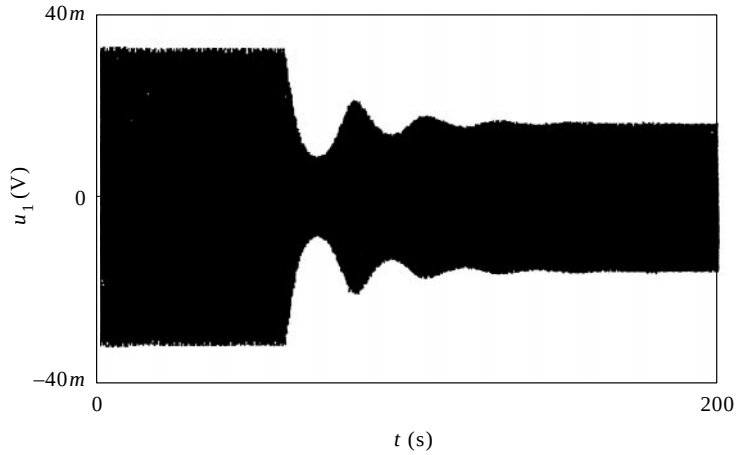

Figure 10. Controller response u_1 in controlling the steady-state first-mode vibration: $g_{11} = 50$ when $0 < t < 60$ s and $g_{11} = 200$ when $60 < t < 200$ s.

In Figure 1, "u2" (i.e. u_2) represents the voltage from the PZT sensor and "u1" (i.e. u_1) represents the controller voltage. Hence "G12*u1*u2" is a direct excitation voltage to "u1". In other words, g_{12} in equation (1) is exactly the same as the gain constant "G12" in the DS1102 controller. On the other hand, "$\hat{F}$*cos (Ωt)" and "G11*u1*u1*40" are indirect excitation voltages to "u2", and they are due to the actuation of the external excitation PZT actuator and the two controlling PZT actuators, respectively. The actuating forces are created by the three PZT actuators, transferred to the structure, and then received by the PZT sensor. It it is a single-mode vibration, the coefficients F and g_{11} in equation (1) can be obtained from "$\hat{F}$", "G11", and one single measured point on the frequency response curve, as explained below (see Appendix for the derivation). When u_2 is not coupled with u_1 (i.e. $g_{11} = g_{12} = 0$), if a voltage $\hat{F} \cos \Omega t$ is applied to the external excitation actuator and the response amplitude of u_2 is measured to be a_2, it follows from the linear vibration theory that the direct excitation voltage F to the PZT sensor is

$$F = a_2 \omega_2^2 \sqrt{\left(1 - \frac{\Omega^2}{\omega_2^2}\right)^2 + \left(2\zeta_2 \frac{\Omega}{\omega_2}\right)^2}, \tag{29}$$

where the modal damping ratio ζ_2 needs to be obtained experimentally. Then g_{11} can be obtained as

$$g_{11} = G11 \times 10 \times 40 \times 2 = 800 \times G11, \tag{30}$$

where the 40 accounts for the use of a power amplifier, and the 2 accounts for the use of two PZT actuators for control. All dSPACE functions which write data to output devices expect their input values lying within the range $-1 \cdots +1$, and they multiply an input signal (voltage) by 10 before it is sent out. Hence, the 10 in equation (30) accounts for this fact.

For the first mode of the beam, ω_2 and ζ_2 are obtained using modal testing to be $\omega_2 = 5{\cdot}85$ Hz and $\zeta_2 = 0{\cdot}0025$, and the output voltage amplitude of the sensor PZT patch is measured to be $a_2 = 0{\cdot}1 \times 47{\cdot}7 = 4{\cdot}77$ V when $\hat{F} = 20$ V and $\Omega = 5{\cdot}85$ Hz. All dSPACE functions which read data from input devices automatically scale their output data to floating-point values lying within the range $-1 \cdots +1$. For the specific case, the scaling factor is 47·7. Then, we obtain from equation (29) that $F = 32{\cdot}22$ V/s^2 and $F/\hat{F} = 1{\cdot}611$

$1/s^2$. Hence, it follows from Figure 1 that the system equations for the control of the first-mode steady-state vibration are

$$\ddot{u}_1 + \omega_1^2 u_1 = G12 \times u_1 u_2,$$

$$47{\cdot}7(\ddot{u}_2 + 0{\cdot}1838\dot{u}_2 + 1351u_2) = \frac{F}{\hat{F}}[G11 \times 800u_1^2 + \hat{F}\cos(\Omega t)]. \tag{31}$$

u_1 is the controller voltage inside the DS1102 controller, u_2 is the sensor voltage inside the DS1102, and $47{\cdot}7u_2$ is the actual sensor voltage. In equation (31) we use the fact that the PZT patch for external excitation and the two PZT patches for control are located at the same position on the x-axis and hence they have the same $F/\hat{F}$. The physical meaning of $F/\hat{F}$ is explained in the Appendix.

A direct numerical integration of equation (31) with initial conditions $\dot{u}_1(0) = 0$ and $u_1(0) = 0{\cdot}02$ has been performed. Figure 3 shows the numerical solution of the first-mode

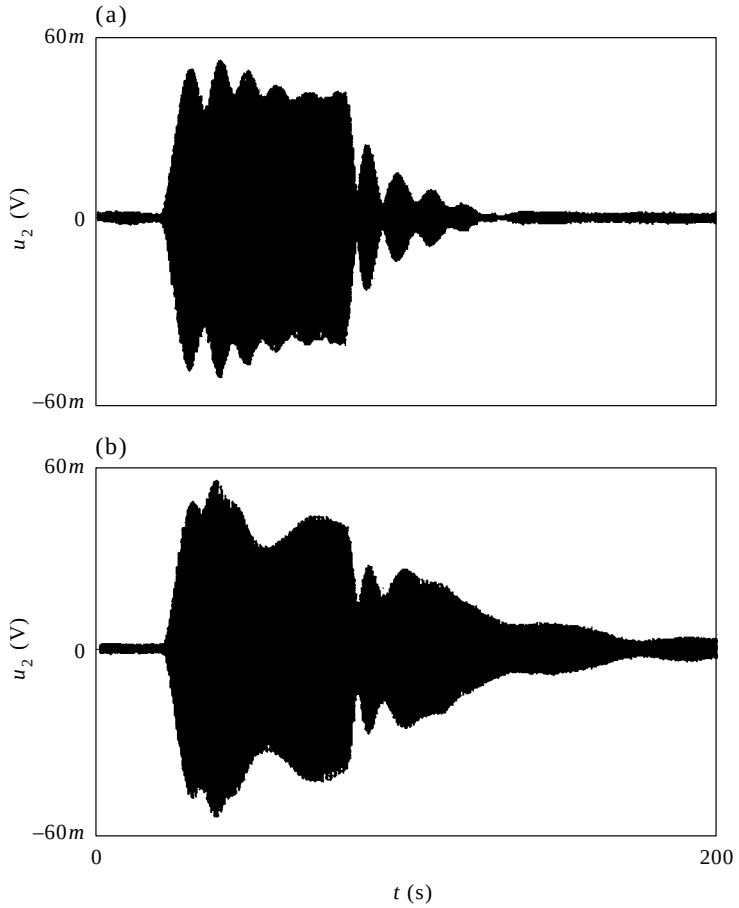

Figure 11. Controlled steady-state first-mode response u_2: (a) $\Omega = 5{\cdot}85$ Hz and $2\omega_1 = 5{\cdot}85$ Hz when $0 < t < 20$ s, $\Omega = 5{\cdot}9$ Hz and $2\omega_1 = 5{\cdot}85$ Hz when $20 < t < 80$ s, and $\Omega = 5{\cdot}9$ Hz and $2\omega_1 = 5{\cdot}9$ Hz when $80 < t < 200$ s; and (b) $\Omega = 5{\cdot}85$ Hz and $2\omega_1 = 5{\cdot}85$ Hz when $0 < t < 20$ s, $\Omega = 5{\cdot}8$ Hz and $2\omega_1 = 5{\cdot}85$ Hz, when $20 < t < 80$ s, and $\Omega = 5{\cdot}8$ Hz and $2\omega_1 = 5{\cdot}8$ Hz when $80 < t < 200$ s.

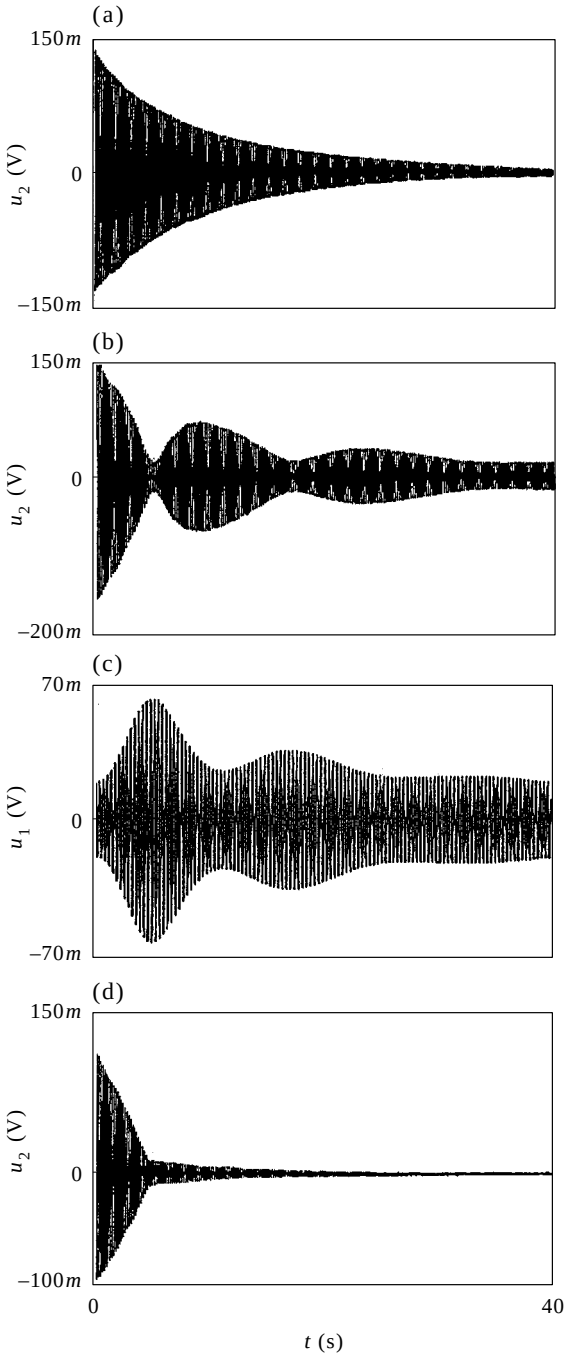

Figure 12. Experimental internal resonance control of the first-mode transient vibration: (a) uncoupled and uncontrolled transient response u_2, (b) coupled but uncontrolled ($\zeta_1 = 0$) transient response u_2, (c) coupled but undamped controller response u_1, and (d) controlled transient response u_2.

steady-state vibration before and after the controller is activated at $t = 50$ s. Figure 4 shows the numerical solution of the internal resonance control of the first-mode transient vibration.

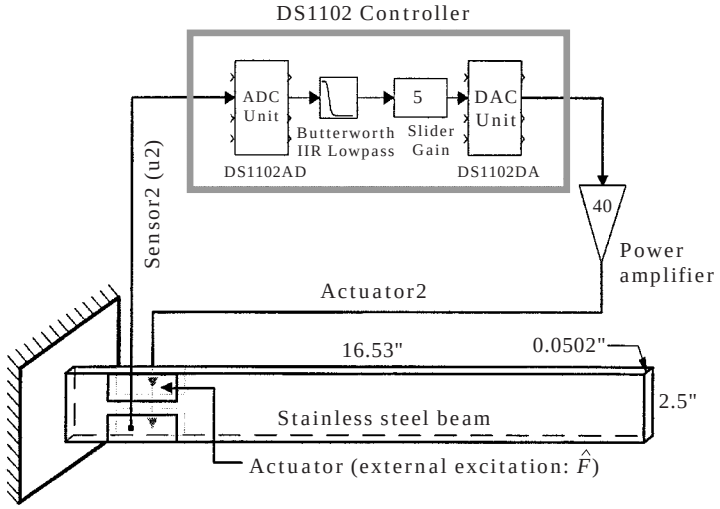

Figure 13. A digital linear position-feedback controller for controlling steady-state and transient vibrations.

5. EXPERIMENTAL RESULTS

5.1. STEADY-STATE VIBRATION CONTROL

Figure 5 shows the sensor and controller responses in controlling the first-mode steady-state vibration where $150\,m \equiv 0{\cdot}150$. Because the buffer size of the DS1102 controller is limited, only one out of every three consecutive data points is downloaded for plotting. The experimental result in Figure 5 agrees closely with the numerical result in Figure 3. Figure 6 shows the first-mode, second-mode, and third-mode steady-state responses before and after control action. In Figure 6(a), the controller was activated at $t = 10$ s. At $t = 100$ s, the controller was deactivated allowing the response to develop, and then the controller was activated again at $t = 120$ s. The results show that the beam vibration is always successfully suppressed after the controller is activated.

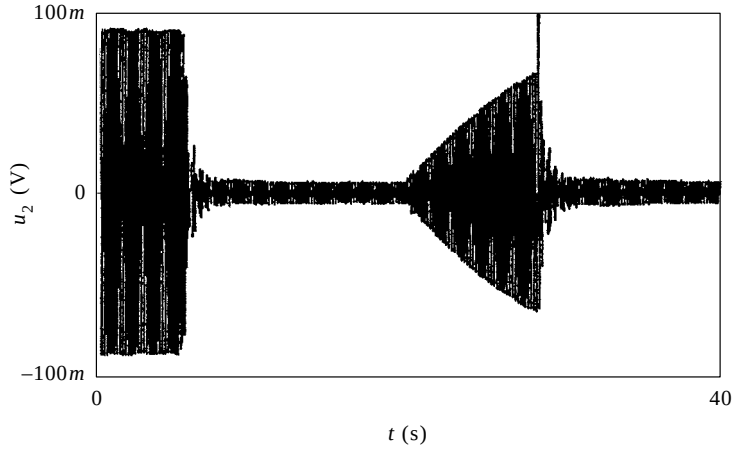

Figure 14. Linear position-feedback control of the steady-state first-mode response u_2 (the controller is on when $5 < t < 20$ s and $28 < t < 40$ s).

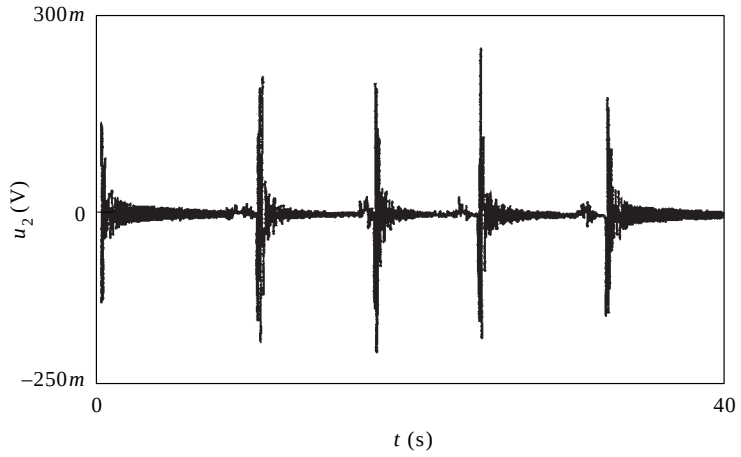

Figure 15. Linear position-feedback control of the first-mode transient response u_2.

The overshooting of the beam response u_2 [see Figures 6(b, c)] at the activation of the controller can be harmful to the structure because it may cause sudden large deformations and hence damage. It is difficult to prevent the overshooting because it is determined by the initial conditions $u_1(0)$ and $\dot{u}_1(0)$, the relative phase between u_2 and u_1^2 when the controller is activated, and the value of g_{11}.

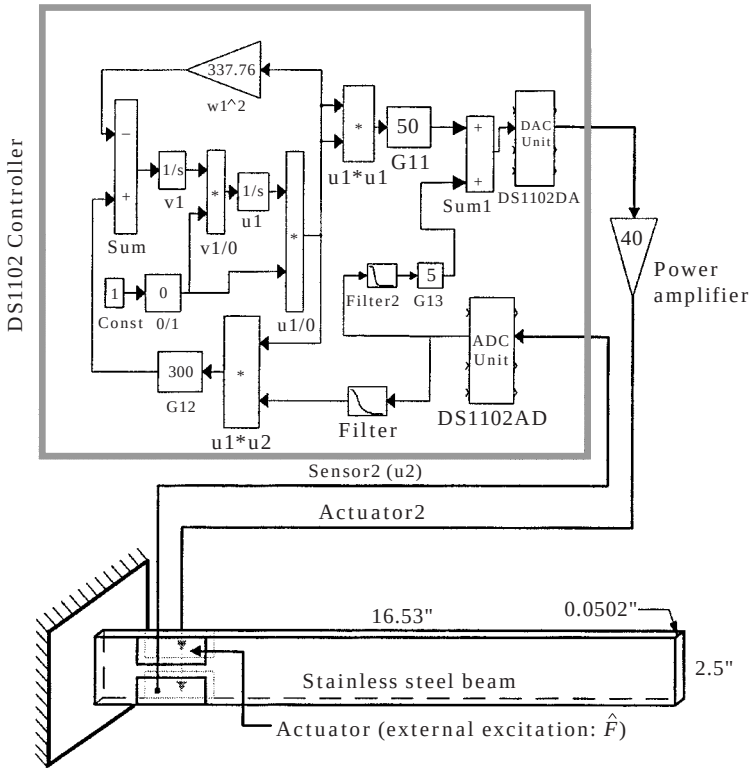

Figure 16. A hybrid controller.

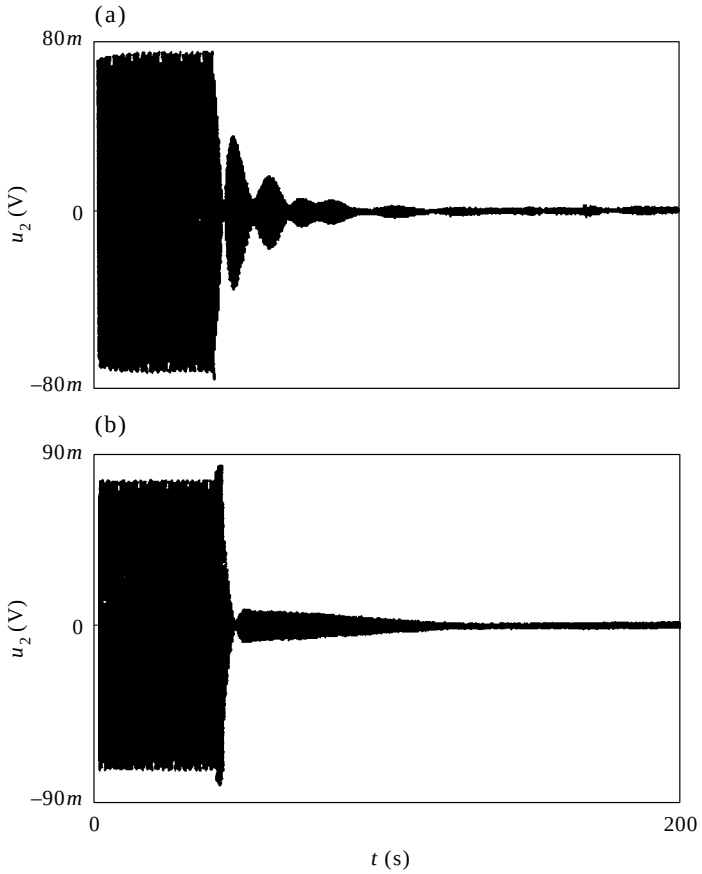

Figure 17. Control of the first-mode steady-state response u_2: (a) using a saturation controller, and (b) using a hybrid controller.

For the first-mode vibration, the uncontrolled tip vibration amplitude is about 0·15″, which is 3 times of the beam thickness. Hence the vibration is not really linear, but this control method still works although the beam is assumed to be linear in the theoretical derivation. To confirm this point, we add geometric non-linearities to equation (31) and consider that

$$\ddot{u}_1 + \omega_1^2 u_1 = G12 \times u_1 u_2,$$

$$47{\cdot}7(\ddot{u}_2 + 0{\cdot}1838\dot{u}_2 + 1351u_2 + \alpha_2 u_2^2 + \alpha_3 u_2^3) = \frac{F}{\hat{F}}[G11 \times 800u_1^2 + \hat{F}\cos(\Omega t)]. \quad (32)$$

The numerical results in Figure 7 confirm that this saturation control method also works for large-amplitude vibrations.

Figure 8 shows that the controlled steady-state amplitude a_2 remains the same if only one PZT control actuator is used instead of using two control actuators. It confirms that a_2 is not a function of the actuation force F. However, one can see by comparing Figures 6(a) and 8 that, when F is small, the transient time required to reach the controlled steady-state vibration increases.

Figure 9 shows the controlled steady-state response u_2 corresponding to different values of g_{12}. It confirms that a_2 is proportional to $1/g_{12}$. Figure 10 shows the controller response u_1 corresponding to different values of g_{11}. It confirms that a_1 is proportional to $1/\sqrt{g_{11}}$.

Figure 11 shows that, when $\Omega - 2\omega_1(\sigma_1 - \sigma_2)$ deviates from zero, a_2 increases. If $\Omega = 2\omega_1$ but Ω is away from ω_2, a_2 stays about the same as that when $\Omega = 2\omega_1 = \omega_2$, which agrees with the perturbation solution. However, the transient time required to reach the steady state increases, and, when Ω is far away from ω_2, a_2 is large because the transient time becomes infinity.

Since equation (19) shows that $g_{11}u_1^2$ contains a d.c. term that may cause static beam deflection, we tried the use of a band-pass filter to filter out this d.c. component as well as high-frequency components. Results show that the efficiency of the modified controller becomes more dependent on the initial conditions and the relative phase between u_2 and u_1^2 when the controller is activated; and the controller becomes unstable in some cases. Hence, the d.c. component in $g_{11}u_1^2$ actually plays a positive role in this control method.

5.2. TRANSIENT VIBRATION CONTROL

The free, coupled but uncontrolled, and controlled transient first-mode responses are shown in Figure 12. Figure 12(a) shows the uncontrolled free first-mode vibation. Figure 12(b, c) show that the vibation energy is transferred back and forth between the

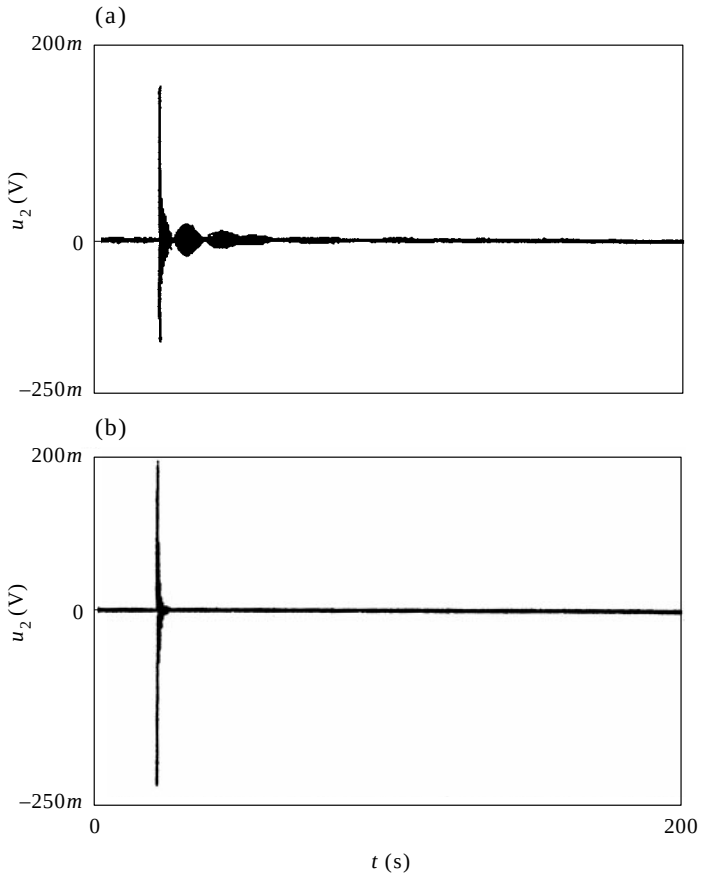

Figure 18. Control of the first-mode steady-state response u_2 with a sudden impact disturbance applied at $t = 20$ s: (a) using a saturation controller, and (b) using a hybrid controller.

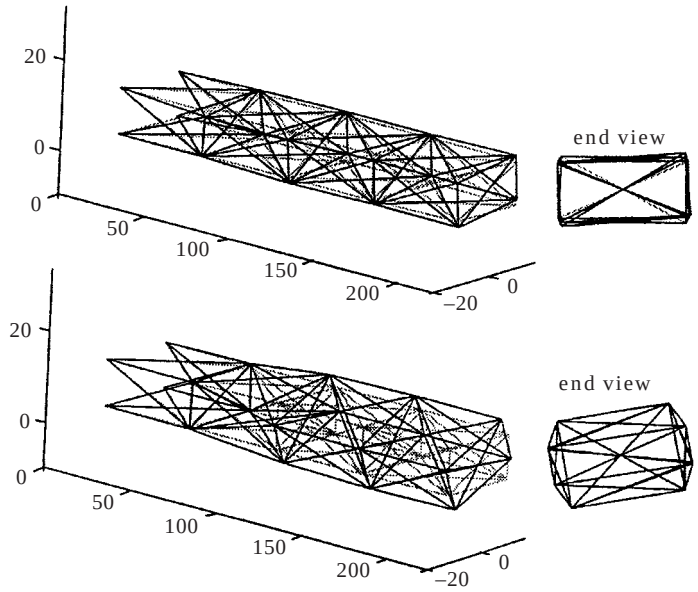

Figure 19. Bi-moment induced twisting of a cantilever truss: (a) a 180° bi-moment on the first bay, and (b) a non-parallel twisting bi-moment on the second bay.

beam and the controller when they are quadratically coupled but the damping of the controller is not on. Figure 12(d) shows the controlled beam response when the beam and the controller are coupled and the damping of the controller is activated at $t = 5$ s.

The numerical results in Figure 4 agree closely with the experimental results in Figure 12. Numerical and experimental results show that this control method is efficient only if the damping in the controller can be activated at the instant when the amplitude of the beam vibration reaches a local minimum. However, it is difficult to predict when the local minimum will happen because it depends on initial conditions. Moreover, if there is a second transient disturbance to the beam, the controller needs to be re-set to a non-zero initial condition in order to work. Hence it is inconvenient.

5.3. DIRECT POSITION-FEEDBACK CONTROL

The saturation and internal resonance control methods can be used to control several modes at the same time by using several such controllers with each controller being designed to control one structural mode. However, since extensive computations are involved in these nonlinear digital controllers, if many such controllers need to be used, the computation speed of the control system may not be able to perform real-time control. Since a linear position-feedback control method is simple in computation, we tried it in controlling the same structure. Figure 13 shows the linear position-feedback controller designed for controlling both transient and steady-state vibrations.

Figure 14 shows the control of the steady-state first-mode vibration. It appears that the transient time required to reach the steady state is very short. However, since the control force directly comes from the beam vibration itself, the controlled vibration amplitude a_2 can never approach zero. Although a_2 can be reduced by using a larger feedback gain, the system becomes unstable when the gain is beyond a certain value (6 for controlling the first mode of this specific system with the chosen filter).

Figure 15 shows the linear position-feedback control of the first-mode transient vibration, where roughly the same amount of initial tip displacement disturbance is given at $t = 0$, 10, 18, 24, and 33 s. Comparing Figure 15 with Figure 12, we found that this controller is much more efficient and robust than the internal resonance controller. However, because filters are always needed in a digital control system and filters always distort and change the phase of the feedback signal in some degree, a linear position-feedback controller is easier to become unstable, especially when a large feedback gain is used. On the other hand, equation (1) shows that the phase of the control force $g_{11}u_1^2$ of the nonlinear controller is not directly affected by the feedback signal u_2. Moreover, the overshooting problem in the linear position-feedback control method seems more serious than that in the internal resonance control method.

5.4. HYBRID CONTROLLER

Since a saturation controller is efficient in controlling steady-state vibrations and a linear position-feedback controller is efficient in controlling transient vibrations, a hybrid controller is designed consisting of one saturation controller to control the major steady-state vibration mode and one linear position-feedback controller to control transient vibrations and other minor steady-state vibration modes, as shown in Figure 16.

Figure 17 shows that the hybrid controller [Figure 17(b)] requires a much less transient time for reaching the controlled steady state than the saturation controller [Figure 17(a)]. Figure 18 shows that the hybrid controller is efficient in controlling steady-state vibrations with sudden disturbances. The experimental results show that the hybrid controller does behave much better than the other controllers.

5.5. DISCUSSIONS

The first torsional frequency of the cantilever beam is estimated to be 115·8 Hz. A 180° bi-moment was tried to excite the first torsional mode, but it was not successful because the thickness is too thin and hence the induced bi-moment is not strong enough to excite the first torsional mode. We used a cantilever truss (see Figure 19) to study the efficiency of 180° bi-moments and non-parallel twisting bi-moments. All the members of this truss have the same cross-section and Young's modulus.

Figure 19(a) shows the twisting of the truss when an induced strain [Λ_1 in equation (27)] of $\pm 0{\cdot}15$ is applied to the four longitudinal members of the first bay. Figure 19(b) shows the twisting of the truss when an induced strain of $\pm 0{\cdot}03$ is applied to the four diagonal members on the top and bottom faces of the second bay. We note that the non-parallel twisting bi-moment is more efficient than the 180° bi-moment. However, beams may not behave exactly the same as trusses in torsion. To understand beam twisting vibrations due to bi-moments, torsional warping deformations need to be analyzed using finite-element methods or other methods. This problem requires more studies.

6. CONCLUDING REMARKS

The use of PZT patches, the nonlinear saturation phenomenon, and internal resonances to control the steady-state and transient vibrations of a cantilever beam has been shown by perturbation analysis, numerical simulation, and experiments. The theoretical and experimental results show that the saturation control of steady-state vibrations is efficient and robust. Although the internal resonance control method works in controlling transient vibrations, it is inconvenient for use and is not as efficient as a simple linear position-feedback control method. A hybrid controller consisting of a saturation controller and a linear position-feedback controller is shown to be robust and efficient in controlling steady-state and transient vibrations.

ACKNOWLEDGMENT

This work is supported by the U.S. Army Research Office under Grant No. DAAH04-96-1-0048. Dr Gary L. Anderson is the technical monitor. The support is gratefully acknowledged.

REFERENCES

1. A. H. Nayfeh and D. T. Mook 1979 *Nonlinear Oscillations*. New York: Wiley.
2. P. F. Pai ad A. H. Nayfeh 1991 *Nonlinear Dynamics* **2**, 1–34. Three-dimensional non-linear vibrations of composite beams—II. Flapwise excitations.
3. M. F. Golnaraghi 1991 *Journal of Dynamics and Control* **1**, 405–428. Regulation of flexible structures via nonlinear coupling.
4. S. S. Oueini and A. H. Nayfeh 1996 *AIAA-96-1642-CP*. Saturation control of a DC motor.
5. S. S. Oueini, A. H. Nayfeh and M. F. Golnaraghi 1997 *Nonlinear Dynamics* **13**, 189–202. A theoretical and experimental implementation of a control method based on saturation.
6. S. S. Oueini and M. F. Golnaraghi 1997 *Journal of Sound and Vibration*, in press. Experimental implementation of the internal resonance control strategy.
7. C. Park, C. Walz and I. Chopra 1993 *The SPIE Smart Structures and Materials* '93, *Alburquerque*, *NM*. Bending and torsion models of beams with induced strain actuators.
8. A. Koike 1994 *Master Thesis*, *Virginia Tech*. Torsional and flexural control of sandwich composite beams with piezoelectric actuators.
9. D. Iesan 1987 *St. Venant's Problem*. Lecture Notes in Mathematics, No. 1279, A. Dold and B. Eckmann, ed. New York: Springer.
10. V. Giavotto, M. Borri, P. Mantegazza, G. Ghiringhelli, V. Carmaschi, G. C. Maffioli and F. Mussi 1983 *Computers & Structures* **16**, 403–413. Anisotropic beam theory and applications.
11. P. F. Pai, B. Wen, A. S. Naser and M. J. Schulz 1997 *AIAA-97-1357-CP*. Nonlinear vibration suppression of cantilever beams using bi-moment induced by PZT actuators.
12. *SIMULINK*: *Dynamic System Simulation Software*. Natick, MA: The MathWorks.
13. dSPACE digital signal processing and control engineering GmbH, Paderborn, Germany.
14. R. M. Mersereau and M. J. T. Smith 1994 *Digital Filtering*: *A Computer Laboratory Textbook*. New York: Wiley.
15. Active Control eXperts, Inc., Cambridge, MA.
16. P. F. Pai, A. H. Nayfeh, K. Oh and D. T. Mook 1993 *International Journal of Solids and Structures* **30**, 1603–1630. A refined nonlinear model of composite plates with integrated piezoelectric actuators and sensors.

APPENDIX: COEFFICIENTS OF EQUATIONS (1)

For a beam with an integrated PZT actuator between x_1 and x_2 (see Figure 1), the equation of motion is given by [16].

$$m\ddot{w} + c\dot{w} + (EIw'')'' = \bar{M}'', \tag{A1}$$

where $w(x, t)$ is the transverse displacement, $(\,)' \equiv \partial(\,)/\partial x$, m is the mass per unit length, E is Young's modulus, I is the area moment of inertia, c is the viscous damping coefficient, and

$$\bar{M} = -k_a V_3(t)(U(x - x_1) - U(x - x_2)). \tag{A2}$$

Here $V_3(t)$ is the voltage applied to the PZT actuator, U is a unit-step function, and k_a is a constant. k_a is a function of piezoelectric constants, mechanical properties, and dimensions of the PZT patch and the beam. To relate k_a to these properties, we assume

that the axial strain ε_{11} distribution (due to the actuation of the PZT patch) of the beam segment covered by the PZT patch is

$$\varepsilon_{11} = -w'' f_a(z), \tag{A3}$$

where $f_a(z)$ is a function that can be determined by using localized analytical or numerical analyses, such as two-dimensional sectional finite-element analyses [10]. Hence

$$\bar{M} = -\int \sigma_{11} z \, \mathrm{d}A = \int E w'' f_a(z) z \, \mathrm{d}A = E\hat{I} w'', \tag{A4}$$

where A is the beam cross section area and $\hat{I} \equiv \int f_a(z) z \, \mathrm{d}A$. The free expansion strain Λ_1 of the PZT patch is reduced to $\hat{k}_a \Lambda_1 (0 < \hat{k}_a < 1)$ because of the straining of the attached beam. Hence, it follows from equations (A3) and (27) that

$$-w'' \hat{f}_a = \hat{k}_a d_{31} \frac{V_3}{t_3}, \tag{A5}$$

where $\hat{f}_a \equiv f_a(h/2)$ and h is the thickness of the beam. Substituting the actuated curvature w'' in equation (A5) into equation (A4) and then comparing with equation (A2) (without considering the locating function), we obtain that

$$k_a \equiv \frac{E\hat{I}\hat{k}_a d_{31}}{\hat{f}_a t_3}. \tag{A6}$$

For a single-mode vibration, we assume that

$$w(x, t) = W(x)\eta(t), \tag{A7}$$

where $\eta(t)$ is one of the modal coordinates of a cantilever beam, and $W(x)$ is one of the eigenfunctions and is given by

$$W(x) = \cosh \beta x - \cos \beta x + \frac{\cos \beta l + \cosh \beta l}{\sin \beta l + \sinh \beta l} (\sin \beta x - \sinh \beta x). \tag{A8}$$

Here l is the beam length, β is one of the solutions of the characteristic equation $\cos \beta l \cosh \beta l + 1 = 0$, and $\beta^4 = m\omega^2/EI$. For this specific eigenfunction, one can prove that

$$\int_0^l W^2 \, \mathrm{d}x = l. \tag{A9}$$

Moreover, since $U'(x - x_n) = \delta(x - x_n)$ (δ is the Kronecker delta function) and $U''(x - x_n) = (\delta(x - x_n) - \delta(x - x_n - \mathrm{d}x))/\mathrm{d}x$, we have

$$\int_0^l W U''(x - x_1) \, \mathrm{d}x = (W(x_1) - W(x_1 + \mathrm{d}x))/\mathrm{d}x$$

$$= (W(x_1) - W(x_1) - W'(x_1) \, \mathrm{d}x)/\mathrm{d}x = -W'(x_1). \tag{A10}$$

Assuming that m, c, and EI are constant, substituting equations (A2) and (A7) into equation (A1), multiplying equation (A1) with $W(x)$, integrating through the whole beam length, and using equation (A9), we obtain that

$$l(m\ddot{\eta} + c\dot{\eta} + m\omega^2\eta) = k_a V_3 (W'(x_1) - W'(x_2)). \tag{A11}$$

We assume that the axial strain ε_{11} distribution (due to the attachment of the PZT sensor) of the beam segment covered by the PZT sensor is

$$\varepsilon_{11} = -w'' f_s(z), \tag{A12}$$

where $f_s(z)$ is a function that can be determined by using localized analytical or numerical analyses, such as two-dimensional sectional finite-element analyses [10]. For a PZT sensor locating between x_3 and x_4, the actual sensed voltage $\hat{u}_2$ [i.e. $47{\cdot}7u_2$ in equation (31)] is given by

$$\hat{u}_2 = g_{31}\sigma_{11}|_{z=h/2} t_3 = -g_{31} E\eta \hat{W}'' \hat{f}_s t_3 = -k_s \eta, \tag{A13}$$

where $\bar{W}'' \equiv \int_{x_3}^{x_4} W'' \, dx/(x_4 - x_3) = (W'(x_4) - W'(x_3))/(x_4 - x_3)$ is the averaged curvature, $\hat{f}_s \equiv f_s(h/2)$, and

$$k_s \equiv g_{31} E \bar{W}'' \hat{f}_s t_3. \tag{A14}$$

Substituting equation (A13) into equation (A11) yields

$$\ddot{\hat{u}}_2 + 2\zeta\omega\dot{\hat{u}}_2 + \omega^2 \hat{u}_2 = -\frac{k_s}{lm} k_a V_3 (W'(x_1) - W'(x_2)), \tag{A15}$$

where $c/m = 2\zeta\omega$ is assumed. In equation (A15), V_3 represents $g_{11}u_1^2$ (the input voltage to the PZT actuators for control). It follows from equations (A15) and (31) that the F and $\hat{F}$ are related as

$$\frac{F}{\hat{F}} = \frac{k_a k_s}{lm} (W'(x_2) - W'(x_1)). \tag{A16}$$